Modelling of a Food Processing Plant for Industrial Demand Side Management

Conference Paper · April 2022

DOI: 10.5281/zenodo.7234548

5 authors, including:

Philipp Wohlgenannt
Fachhochschule Vorarlberg
2 PUBLICATIONS **0** CITATIONS
SEE PROFILE

Klaus Rheinberger
Fachhochschule Vorarlberg
40 PUBLICATIONS **882** CITATIONS
SEE PROFILE

Markus Preissinger
Fachhochschule Vorarlberg
47 PUBLICATIONS **1,182** CITATIONS
SEE PROFILE

Peter Kepplinger
Fachhochschule Vorarlberg
34 PUBLICATIONS **336** CITATIONS
SEE PROFILE

Modelling of a Food Processing Plant for Industrial Demand Side Management

P. Wohlgenannt[1,2], G. Huber[1], K. Rheinberger[1], M. Preißinger[1], P. Kepplinger[1*]

[1]Josef Ressel Centre for Intelligent Thermal Energy Systems,
illwerke vkw Endowed Professorship for Energy Efficiency, Research Center Energy,
Vorarlberg University of Applied Sciences, Hochschulstrasse 1, 6850 Dornbirn, Austria

[2]Faculty of Engineering and Science, University of Agder, 4879 Grimstad, Norway

*Corresponding author: peter.kepplinger@fhv.at

Abstract

Industrial demand side management has shown significant potential to increase the efficiency of industrial energy systems via flexibility management by model-driven optimization methods. We propose a grey-box model of an industrial food processing plant. The model relies on physical and process knowledge and mass and energy balances. The model parameters are estimated using a predictive error method. Optimization methods are applied to separately reduce the total energy consumption, total energy costs and the peak electricity demand of the plant. A viable potential for demand side management in the plant is identified by increasing the energy efficiency, shifting cooling power to low price periods or by peak load reduction.

Keywords: Grey-box Model, Processed Food Plant, Industrial Demand Side Management, Intelligent Thermal Energy System

Nomenclature

Physical Quantities

α	absorptance
$\dot{m}$	mass flow rate (kg/s)
$\dot{Q}$	heat transfer rate (W)
η	thermal efficiency
ε	coefficient of performance
ξ	mass flow ratio
C	thermal capacity (J/K)
c	specific thermal capacity (J/(kg K))
h	specific enthalpy (J/kg)
k	overall heat transfer coefficient (W/K)
P	power (W)
p	pressure (bar)
T	temperature (K)
t	time (s)

Further Symbols

π	price function (€/kWh)
N	number of differential equations
N_P	number of process steps
N_T	number of time steps

Subscripts and Abbreviations

∞	ambient
B	building envelope
B2∞	building envelope to ambient
B2P	building envelope to production hall
C	chiller
El	electric
end	end value
F	feed water tank
G	gas
H,C	cooling hall
H,P	production hall
i	discrete time step index
P	product
P2C	production hall to cooling hall
S	steam
S,B	boiler steam
S,E	exhaust vapour
S,F	feed water tank steam
S,H,P	production hall steam
S,P	product steam
W,F	feed water
W,O	osmosis water
W,R	raw water
W,S	softened water

Introduction and Background

Demand side management (DSM) is a promising approach to increase energy system efficiency and to enable the integration of renewable energies into the existing power grid [1]. To reach the full potential of DSM, application in all three consumer sectors is necessary: residential, commercial and industrial. So far, researchers have focused on the residential and the commercial sector [2]. Four main challenges of industrial DSM were identified by Zhang and Grossmann [3]: 1) accurate modelling of operational flexibility; 2) integration of production and energy management; 3) optimization across multiple time scales; 4) decision making under uncertainty.

For the realization of DSM, thermal energy storages are showing a high potential with the ability to shift electric loads from high demand to low demand hours [4, 5, 6]. Arteconi and Polonara [7] reviewed demand side management in refrigeration applications. Different DSM categories (energy efficiency, energy storage and demand response) are discussed and the potential of DSM with chillers and heat pumps in combination with active or passive energy storages is shown.

Shafiei et al. [8] proposed a non-linear model of a supermarket refrigeration system for DSM. They focused on estimating the power consumption of the chillers while estimating the cold reservoirs as well. As DSM method, direct load control is used.

Mueller et al. [9] modelled a set of large industrial freezer warehouse units to act as flexible loads in a smart grid setting. As DSM method, power reference tracking is used. Disturbances like the weather were neglected. The chillers were controlled via temperature set points, a direct compressor control was not implemented. The authors successfully have shown that large freezer systems can be used as flexible loads.

Kepplinger et al. [10] presented an overview of different DSM approaches. Autonomous demand side management methods were applied to different areas such as electric vehicle charging, battery storage systems or domestic hot water storages. In [11], Kepplinger et al. proposed a grey-box modelling approach based on energy and mass balances for thermal systems and DSM methods for optimal predictive control.

We contribute to the first main challenge by proposing a grey-box model of a real industrial plant to serve as the basis for DSM algorithms. In contrast to the papers mentioned above, we present a model of a real processed food plant including the food production process and the refrigeration systems. A linear temperature model is set up such that the effect of controlling the electric power of both chillers can be simulated, making the model well suited for optimization and DSM methods. As only limited data of this system is available via data acquisition, simplifications are made and a grey-box modelling approach is applied. Using methods from Kepplinger et al. [11], the system is described via energy balances, and the parameters are estimated using a predictive error method. As proof of concept, optimal predictive control of the chillers under three DSM scenarios is evaluated: 1) minimization of the total energy consumption; 2) minimization of the total energy costs under real-time pricing; 3) peak load reduction.

Methods

Figure 1 shows a simplified sketch of the plant. The building is divided into three subparts, the production hall, the cooling hall and the thermal mass of the building envelope. The system temperatures are depended on the heat loss of these production lines, the outside temperature, the radiation of the sun and the extracted heat by the two chillers. The first chiller is used for

cooling the production hall and the second one is used for cooling the product in the cooling hall. In this chapter, the production process is first described. Next, the models of the steam boiler and the chillers are described, which serve as inputs for the thermal model. Finally, the analytical solution of the energy balances of the thermal model is used to formulate different optimization-based DSM strategies.

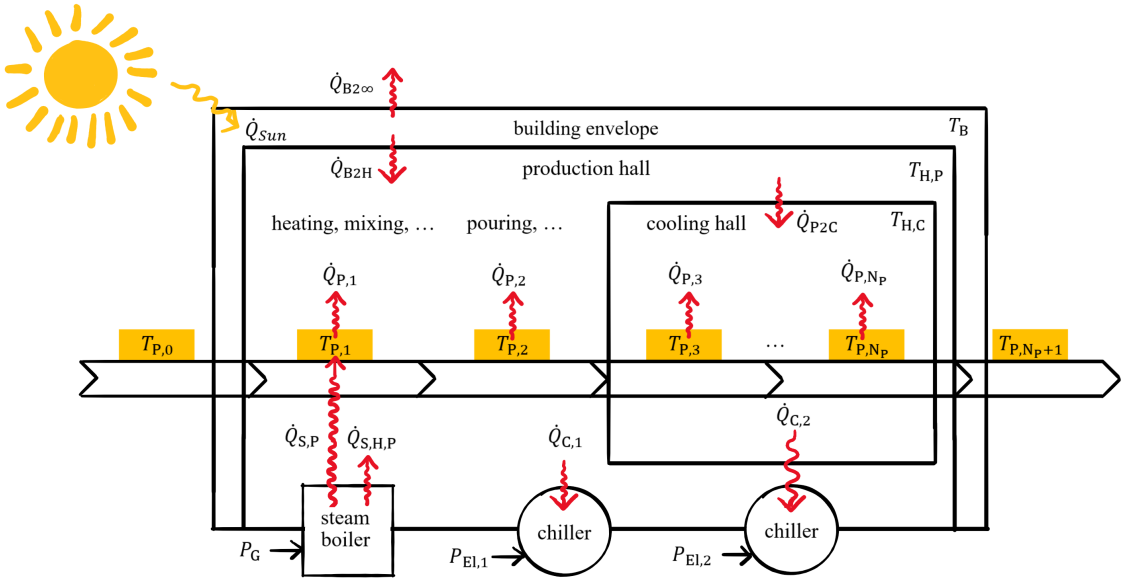

Figure 1. Processed food plant.

The production of processed food is described in detail elsewhere [12, 13, 14]. Here, this batch process is simplified into three different stages: 1) steam ($\dot{Q}_{S,P}$) heats the product to approximately 90 °C (range: 70-130 °C) and served ingredients are mixed in; 2) the fluid product is poured into molds and transported to the cooling room while it cools down; 3) the product is cooled down to approximately 5 °C for storing.

A steam boiler plant provides the steam needed. Figure 2 shows the main components and mass flows in the steam generation system. Only the freshwater ($\dot{m}_{W,R}$) and the steam produced by the boiler ($\dot{m}_{S,B}$) are known by measurement. Therefore a model of the steam generation system is created to estimate the steam $\dot{m}_S$, which is available for production. Due to the direct steam heating of the product, the amount of condensate can be assumed to be negligible as most of the steam is generated from freshwater. First, the freshwater is filtered with a reverse osmosis system, next, Ca^{++} and Mg^{++} ions are filtered out of the remaining permeate ($\dot{m}_{W,O}$). Then softened water ($\dot{m}_{W,S}$) can be used for steam generation. In a feed water tank, the softened water is heated up from $T_{W,S}$=12 °C to T_F=105 °C to achieve full degassing of O_2 and CO_2. Exhaust vapour ($\dot{m}_{S,E}$) is released to the surroundings. The steam boiler heats the feed water ($\dot{m}_{W,F}$) to T_B=175 °C and p_B=9 bar with natural gas ($\dot{Q}_G$). A part of the feed water is used for desalination and blowdown. The resulting steam ($\dot{m}_{S,B}$) is in part used for the heating of the feed water tank ($\dot{m}_{S,F}$), and mostly for production ($\dot{m}_S$).

The feed water tank is assumed to be in steady-state conditions, i.e. $\dot{m}_{S,E}$ being constant. Enthalpies for the states of the fluid, i.e. $h_{W,S}$, $h_{W,F}$ and h_S, are taken from literature [15]. All

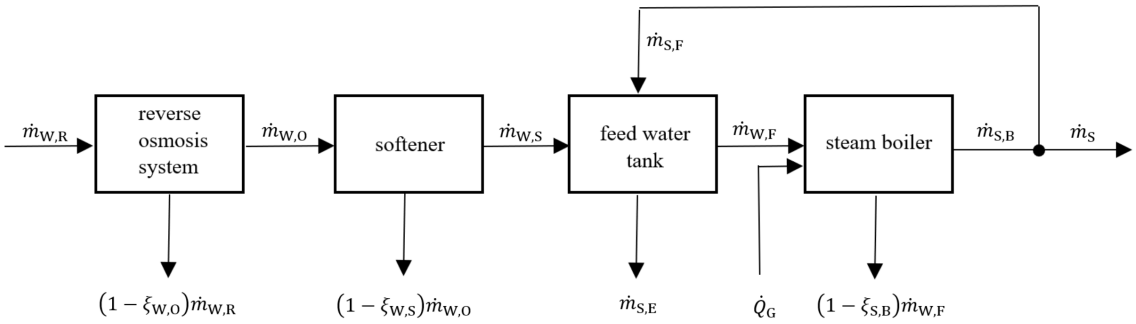

Figure 2. Steam generation system.

mass flows can then be derived from $\dot{m}_{\mathrm{S}}$ using mass and energy balances as follows:

$$\dot{m}_{\mathrm{W,O}} = \dot{m}_{\mathrm{W,R}}\xi_{\mathrm{W,O}} \tag{1}$$
$$\dot{m}_{\mathrm{W,S}} = \dot{m}_{\mathrm{W,O}}\xi_{\mathrm{W,S}} \tag{2}$$
$$\dot{m}_{\mathrm{W,F}} + \dot{m}_{\mathrm{S,E}} = \dot{m}_{\mathrm{W,S}} + \dot{m}_{\mathrm{S,F}} \tag{3}$$
$$\dot{m}_{\mathrm{S,B}} = \dot{m}_{\mathrm{W,F}}\xi_{\mathrm{S,B}} \tag{4}$$
$$\dot{m}_{\mathrm{S,B}} = \dot{m}_{\mathrm{S}} + \dot{m}_{\mathrm{S,F}} \tag{5}$$
$$\dot{m}_{\mathrm{W,F}}h_{\mathrm{W,F}} + \dot{m}_{\mathrm{S,E}}h_{\mathrm{S,E}} = \dot{m}_{\mathrm{W,S}}h_{\mathrm{W,S}} + \dot{m}_{\mathrm{S,F}}h_{\mathrm{S}} \tag{6}$$
$$\dot{m}_{\mathrm{W,F}}h_{\mathrm{W,F}} + \dot{Q}_{\mathrm{G}} = \dot{m}_{\mathrm{S,B}}h_{\mathrm{S}} \tag{7}$$
$$\dot{Q}_{\mathrm{G}} = \eta P_{\mathrm{G}} \tag{8}$$

During times of no production, i.e. $\dot{m}_{\mathrm{S}} = 0$, $\dot{m}_{\mathrm{S,E}}$ can be calculated. Typical values for $\xi_{\mathrm{W,O}}$, $\xi_{\mathrm{W,S}}$ and $\xi_{\mathrm{S,B}}$ and the thermal efficiency η of a steam boiler are provided in literature [16]. Using $\dot{m}_{\mathrm{S}}$, the heat flow available for production ($\dot{Q}_{\mathrm{S}}$), the heat flow of the steam to the product ($\dot{Q}_{\mathrm{S,P}}$) and the heat flow of the steam to the production hall ($\dot{Q}_{\mathrm{S,H,P}}$) can be calculated by

$$\dot{Q}_{\mathrm{S}} = \dot{m}_{\mathrm{S}}h_{\mathrm{S}}, \tag{9}$$
$$\dot{Q}_{\mathrm{S,P}} = \dot{Q}_{\mathrm{S}}\xi_{\mathrm{S,P}}, \text{ and} \tag{10}$$
$$\dot{Q}_{\mathrm{S,H,P}} = \dot{Q}_{\mathrm{S}}\xi_{\mathrm{S,H,P}}, \text{ where} \tag{11}$$
$$0 \leq \xi_{\mathrm{S,P}} + \xi_{\mathrm{S,H,P}} \leq 1, \tag{12}$$
$$0 \leq \xi_{\mathrm{S,P}} \leq 1, \text{ and} \tag{13}$$
$$0 \leq \xi_{\mathrm{S,H,P}} \leq 1. \tag{14}$$

Knowing the temperature of the product before and after heating, $\xi_{\mathrm{S,P}}$ can be estimated. $\xi_{\mathrm{S,P}}$ and $\xi_{\mathrm{S,H,P}}$ sum up to less than 100 %, because the excess steam is used to heat offices via a thermal storage.

The cooling power of the chillers is calculated by using the linearized coefficients of performance (COPs) ε_1 and ε_2:

$$\dot{Q}_{\mathrm{C},1} = P_{\mathrm{El},1}\varepsilon_1 \tag{15}$$
$$\dot{Q}_{\mathrm{C},2} = P_{\mathrm{El},2}\varepsilon_2 \tag{16}$$
$$\varepsilon_1(T_\infty) = a_1 T_\infty + b_1 \tag{17}$$
$$\varepsilon_2(T_\infty) = a_2 T_\infty + b_2 \tag{18}$$

The influence of the sun is modelled via the absorbed radiation of the sun ($\alpha \dot{Q}_{\text{Sun}}$) which heats the thermal capacity of the building envelope. The heat transfer rates from the building envelope to production hall and the surroundings are modelled via a single heat transfer coefficient to reflect convection.

Combing this, the energy balances for Figure 1 can be written as:

$$\dot{T}_{\text{B}}(t) = \frac{1}{C_{\text{B}}}\Big[\alpha \dot{Q}_{\text{Sun}}(t) + k_{\text{B2}\infty}\big(T_{\infty}(t) - T_{\text{B}}(t)\big) + k_{\text{B2P}}\big(T_{H,P}(t) - T_{\text{B}}(t)\big)\Big] \tag{19}$$

$$\begin{aligned}\dot{T}_{\text{H,P}}(t) = \frac{1}{C_{\text{H,P}}}\Big[&\dot{Q}_{\text{S,H,P}}(t) - \dot{Q}_{\text{C},1}(t) + k_{\text{B2P}}\big(T_{\text{B}}(t) - T_{\text{H,P}}(t)\big) + k_{\text{P2C}}\big(T_{\text{H,C}}(t) - T_{\text{H,P}}(t)\big) \\ &+ \sum_{n=1}^{2} k_{\text{P},n}\big(T_{\text{P},n}(t) - T_{\text{H,P}}(t)\big)\Big]\end{aligned} \tag{20}$$

$$\dot{T}_{\text{H,C}}(t) = \frac{1}{C_{\text{H,C}}}\Big[- \dot{Q}_{\text{C},2}(t) + k_{\text{P2C}}\big(T_{\text{H,P}}(t) - T_{\text{H,C}}(t)\big) + \sum_{n=3}^{\text{N}_\text{P}} k_{\text{P},n}\big(T_{\text{P},n}(t) - T_{\text{H,P}}(t)\big)\Big] \tag{21}$$

$$\dot{T}_{\text{P},n}(t) = \begin{cases} \frac{1}{C_{\text{P},n}}\Big[\dot{Q}_{\text{S,P}}(t) + k_{\text{P},n}\big(T_{\text{H,P}}(t) - T_{\text{P},n}(t)\big)\Big], & n = 1 \\ \frac{1}{C_{\text{P},n}} k_{\text{P},n}\big(T_{\text{H,P}}(t) - T_{\text{P,n}}(t)\big), & n = 2 \\ \frac{1}{C_{\text{P},n}} k_{\text{P},n}\big(T_{\text{H,C}}(t) - T_{\text{P,n}}(t)\big), & 3 \leq n \leq \text{N}_\text{P} \end{cases} \tag{22}$$

Assuming $\dot{Q}_{\text{Sun}}(t)$, $\dot{Q}_{\text{C},1}(t)$, $\dot{Q}_{\text{C},2}(t)$, $\dot{Q}_{\text{S,H,P}}(t)$, $\dot{Q}_{\text{S,P}}(t)$ and $T_{\infty}(t)$ to be constant in each time interval of the batch process, this defines a system of first-order inhomogeneous linear differential equations with constant coefficients:

$$\dot{\mathbf{T}}(t) = \mathbf{A} \cdot \mathbf{T}(t) + \mathbf{b} \tag{23}$$

$$\forall t \in [t_i, t_{i+1}] \tag{24}$$

This system of differential equations can be solved using the eigenvectors $\mathbf{v}_n$ and the eigenvalues λ_n of the matrix $\mathbf{A}$, expressing $\mathbf{T}(t)$ by coefficient functions $f_n(t)$ and by coefficients g_n,

$$\mathbf{T}(t) = \sum_{n=1}^{N} f_n(t)\mathbf{v}_n \text{ and} \tag{25}$$

$$\mathbf{b} = \sum_{n=1}^{N} g_n \mathbf{v}_n. \tag{26}$$

The solution for this system of equations is given by

$$f_n(t) = f_n(0)e^{\lambda_n t} - \frac{g_n}{\lambda_n}(1 - e^{\lambda_n t}). \tag{27}$$

This analytical solution allows for the calculation of the system dynamics forward in time for a single time interval and can be discretized assuming piecewise constant parameters on N_{T} intervals of duration Δt. The discretized model is used as the basis for the parameter estimation via a prediction error method and the formulation of the optimization problems.

Assuming that the production hall and the cooling hall are controlled via P-controllers, the parameters of the model are estimated by minimizing the quadratic error of the measured and the simulated cooling powers.

Optimal chiller control can be achieved by solving a linear optimization problem. Assuming the price function π and the uncertainties (steam, mass flow of the product, radiation of the sun and outside temperature) to be perfectly known in advance, the optimization problem, which minimizes the total costs for cooling, can be formulated as follows, keeping the production hall and the cooling hall temperature in a set temperature band:

$$\min_{P_{\text{El},1}, P_{\text{El},2}} \sum_{i=1}^{N_\text{T}} (P_{\text{El},1}^{(i)} + P_{\text{El},2}^{(i)}) \pi^{(i)} \tag{28}$$

$$\text{s.t. } \forall i \in [1, ..., N_\text{T}] : \tag{29}$$

$$\dot{\mathbf{T}}^{(i)}(t) = \mathbf{A}^{(i)} \cdot \mathbf{T}^{(i)}(t) + \mathbf{b}^{(i)} \tag{30}$$

$$0 \leq P_{\text{El},1}^{(i)} \epsilon_1 \leq \dot{Q}_{\text{max},1} \tag{31}$$

$$0 \leq P_{\text{El},2}^{(i)} \epsilon_2 \leq \dot{Q}_{\text{max},2} \tag{32}$$

$$T_{\text{H,P,min}} \leq T_{\text{H,P}}^{(i)} \leq T_{\text{H,P,max}} \tag{33}$$

$$T_{\text{H,C,min}} \leq T_{\text{H,C}}^{(i)} \leq T_{\text{H,C,max}} \tag{34}$$

$$T_{\text{H,P}}^{(N_\text{T})} = T_{\text{H,P,end}} \tag{35}$$

$$T_{\text{H,C}}^{(N_\text{T})} = T_{\text{H,C,end}} \tag{36}$$

Using a constant price $\pi = 1$, the energy minimization problem is solved fulfilling the same constraints (29-36),

$$\min_{P_{\text{El},1}, P_{\text{El},2}} \sum_{i=1}^{N_\text{T}} (P_{\text{El},1}^{(i)} + P_{\text{El},2}^{(i)}). \tag{37}$$

To solve the peak load reduction problem, using the same constraints (29-36), the following objective function is defined,

$$\min_{P_{\text{El},1}, P_{\text{El},2}} \max_i P_{\text{El},1}^{(i)} + P_{\text{El},2}^{(i)}. \tag{38}$$

The objective function (38) can be linearized by introducing auxiliary variables.

Results and Discussion

Only limited data from the real factory is available. The electric power consumption of both chillers, the COP of one chiller, the mass flows $\dot{m}_\text{W}$ and $\dot{m}_\text{S}$, the states (temperature or pressure) of the steam boiler systems and the production quantity per day are known. For the outside temperature and the direct radiation of the sun, data from a weather station nearby is used [17].

Table 2 shows the steam boiler parameters estimated.

$\xi_{\text{W,O}}$	$\xi_{\text{W,S}}$	$\xi_{\text{S,B}}$
0.75	0.97	0.90

Table 1. Estimated steam boiler parameters.

The COP of the first chiller is fitted with linear regression from measured data and the COP of the second chiller is calculated using its datasheet [18]. Both are linearized around the operation temperature set point of 20°C.

	a	b
chiller 1	-0.10000	33.6150
chiller 2	-0.03723	14.7674

Table 2. Estimated chiller parameters.

Using equations (1-8), all heat and mass flows of the steam boiler are calculated from $\dot{m}_{\mathrm{S,B}}$, as shown in the left subplot of Figure 3. For better visibility, the data is filtered by applying a moving average filter (window length 3.75 h for $\dot{m}_{\mathrm{S,B}}$ and 7.5 h for $\dot{m}_{\mathrm{W,R}}$). $\dot{m}_{\mathrm{S,B}}$ denotes the measured boiler steam. $\dot{m}_{\mathrm{S}}$ can be used for production and $\dot{m}_{\mathrm{S,F}}$ is lead back to supply the feed water tank. The model is validated by comparing the calculated quantity of freshwater to the recorded values as shown in the right subplot of Figure 3 and resulting in a root mean square error of 0.12 kg/s.

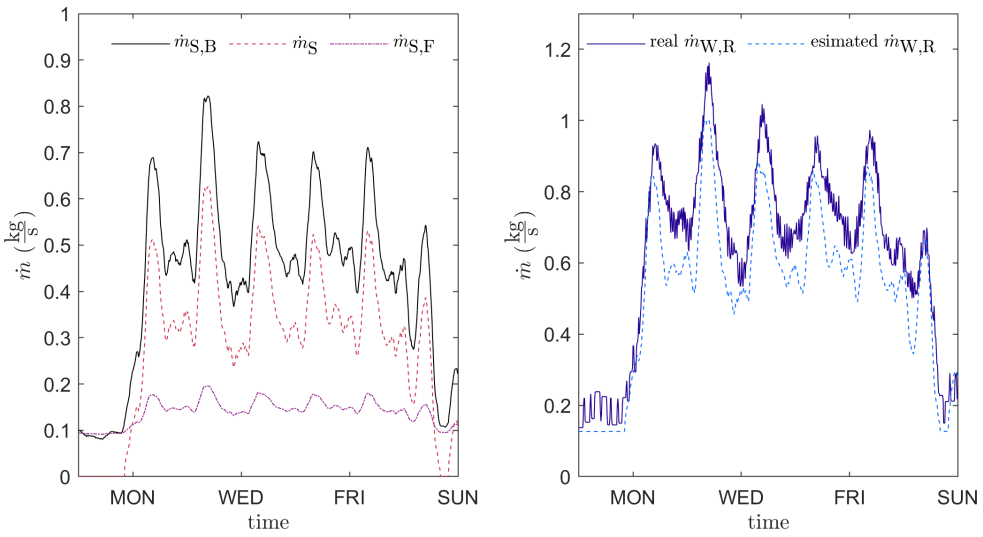

Figure 3. Mass flows of the generated steam, comparison of the estimated and the measured freshwater.

The data is preprocessed to create a single week dataset consisting of average weekdays and average weekends. This data is used to determine the model parameters and the DSM potential. The product mass flow is estimated from the mass flow of the steam, assuming a direct proportion.

The model parameter identification is done using Matlab's [19] *lsqcurvefit* routine. The value of the specific thermal heat coefficient of the product is taken from literature [20]. First the heat transfer coefficients of the product ($k_{\mathrm{P},n}$) and the production steam rate $\xi_{\mathrm{S,P}}$ are fitted such that the heating and cooling time of the product fit measurements. Then, the remaining heat transfer coefficients and thermal capacities from Table 3 are fitted by minimizing the quadratic errors of both chiller powers. The sun has a delayed effect on the system, which is accounted for by the thermal capacity of the building envelope C_{B}. Given temperature bands for the production and the cooling hall, both flexibilities can roughly be estimated using the thermal capacities $C_{\mathrm{H,P}}$ and $C_{\mathrm{H,C}}$. As time interval Δt=30 min and as process step number N_{P}=18 are chosen resulting in a total process time of 9 hours for producing (1 h) and cooling (8 h) for a batch of product and up to 18 possible parallel processes, which are time-shifted by multiples of Δt.

The control of the chillers is simulated with two P-controllers. Figure 4 compares the simulated

parameter	value
$C_{\mathrm{H,P}}$	$3.9 \cdot 10^8 \frac{\mathrm{J}}{\mathrm{K}}$
$C_{\mathrm{H,C}}$	$9.6 \cdot 10^7 \frac{\mathrm{J}}{\mathrm{K}}$
C_{B}	$1.6 \cdot 10^9 \frac{\mathrm{J}}{\mathrm{K}}$
$c_{\mathrm{P},n}$	$3270 \frac{\mathrm{J}}{\mathrm{kg\,K}}$
$k_{\mathrm{B2}\infty}$	$1.3 \cdot 10^4 \frac{\mathrm{W}}{\mathrm{K}}$
k_{B2P}	$1.3 \cdot 10^4 \frac{\mathrm{W}}{\mathrm{K}}$
k_{P2C}	$3.0 \cdot 10^3 \frac{\mathrm{W}}{\mathrm{K}}$
$k_{\mathrm{P},n}$	$0.35 \frac{\mathrm{W}}{\mathrm{kg\,K}} \cdot m_{\mathrm{P},n}$
α	0.98
$\xi_{\mathrm{S,P}}$	0.35
$\xi_{\mathrm{S,H,P}}$	0.05

Table 3. Estimated model parameters.

to the real cooling powers and shows the temperature profile of the production hall and the cooling hall. Figure 5 shows the temperature of a batch of product during the process.

Three different DSM algorithms are applied to the model: 1) an energy-efficient strategy minimizes the total electric power consumption by shifting cooling power to increase the system efficiency 2) a real-time pricing (RTP) strategy minimizes the costs of the electric power by shifting cooling power to low price periods; 3) a peak load reduction strategy minimizes the peak electricity demand. For RTP, the EXAA spot market price [21] is used. The temperature band for the production hall and the cooling hall are chosen to be [15°C, 25°C] and [-6°C, 4°C], respectively. The optimization problems are solved using Matlab's [19] *fmincon* routine for a simulation period of one week. The computations last approximately two days on a laptop with an Intel Core i5 10th Gen. processor.

Table 4 and Figure 6 show the optimal predictive control of the chillers during the different operation modes simulated. As expected, during the energy-efficient mode the temperatures are near the upper boundary to reduce the needed cooling power. Shifting of the cooling power to high chiller efficiency periods during the night can not be observed, because this would have decreased the system efficiency due to the lower temperatures and thereby increased heat flows to the surroundings. The energy reduction also results in a cost reduction. The RTP-driven operation mode reduces the costs by shifting cooling power to low price periods during the night and avoiding price peaks during the day. The costs for the first chiller are reduced by 17 % and the costs of the second chiller are reduced by 10 %. The higher cost reduction achieved by the production hall chiller is due to the high thermal capacity of the production hall. The amount of precooling in the cooling hall is often limited by the cooling hall capacity, as can be seen in the temperature profile when the temperature reaches the lower limit. Due to the better coefficient of performance of the chillers during the night, this mode also reduces the total energy consumption. Finally, a peak load reduction of 21 % is achieved by precooling during the night.

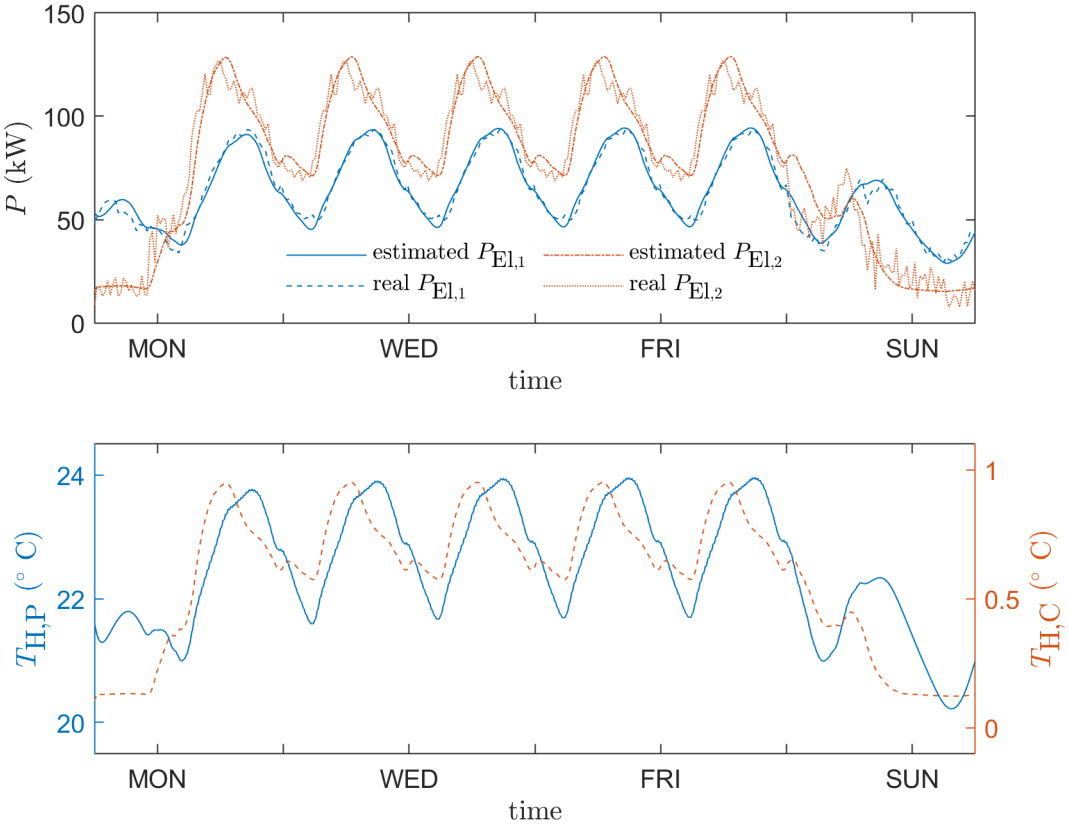

Figure 4. Comparison of the estimated and measured cooling powers (top), temperature profiles of the production hall and the cooling hall (bottom).

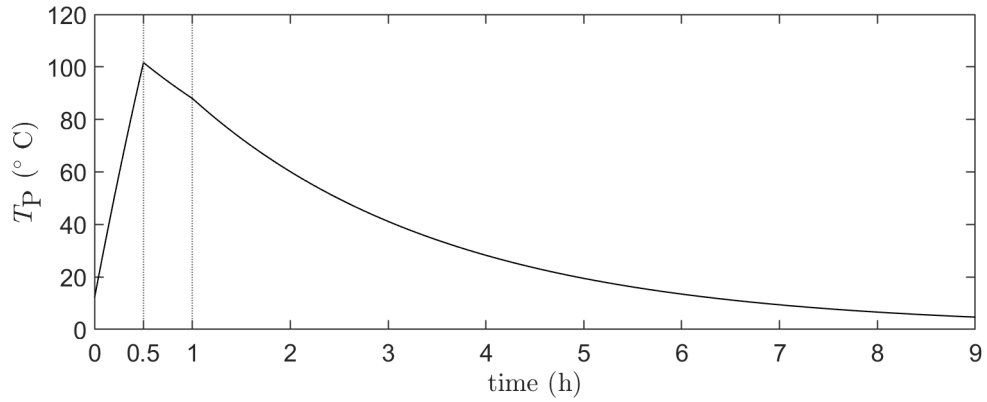

Figure 5. Temperature profile of product during the batch process. The vertical lines indicate the different steps during the batch process, starting with the heating and mixing, next the pouring, and, finally, the cooling.

operation mode		reference	energy-efficient DSM	RTP-driven DSM	peak load reduction
energy per week	total	23.74 MWh	22.71 MWh	23.42 MWh	23.90 MWh
	chiller 1	10.77 MWh	10.19 MWh	10.65 MWh	11.32 MWh
	chiller 2	12.96 MWh	12.52 MWh	12.77 MWh	12.58 MWh
costs per week	total	773 €	743 €	668 €	785 €
	chiller 1	343 €	328 €	283 €	370 €
	chiller 2	430 €	415 €	386 €	415 €
peak power	total	217 kW	216 kW	271 kW	171 kW

Table 4. Optimization results for one simulated week.

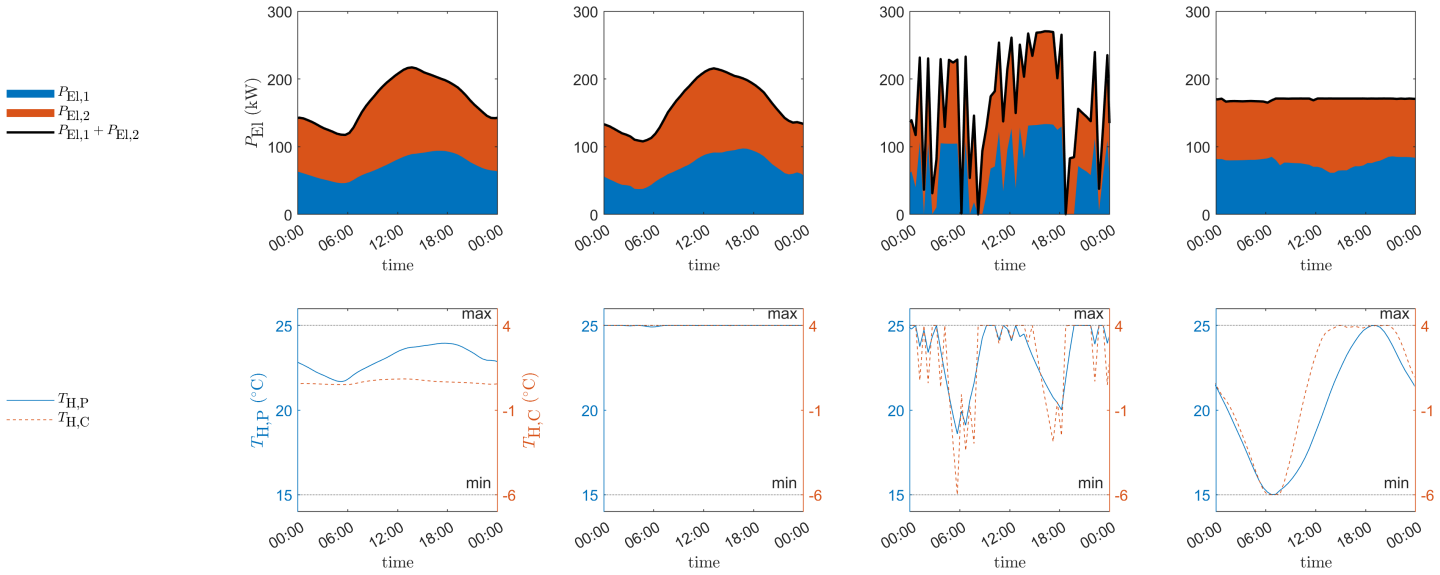

Figure 6. Optimization results for one simulated week, showing the electric power consumption of the two chillers (top) and the production and cooling hall temperatures (bottom). Form left to right: reference case, energy-efficient DSM, RTP-driven DSM, and peak load reduction.

Conclusion and Outlook

A grey-box model of a real industrial food processing plant has been created, whose model parameters were identified by a predictive error method. The method proposed solved the first main challenge of industrial DSM by providing a suitable model. The model was used for optimization-based DSM in a simulation study of one week using Matlab. Austrian day-ahead prices were used for an RTP-driven optimization showing a cost reduction of 14 %. An energy-efficient strategy was able to reduce the energy consumption by 4 % by increasing the temperature to the upper boundary of the allowed range. The peak load could be reduced by 21 % by precooling during the night. Based on the promising DSM potential, future measurements should be established to improve the quality of the estimation of the system dynamics. In further work, this model can be used as the basis for more efficient optimization methods and should deal with challenges like optimization across multiple time scales and decision making under uncertainty.

Acknowledgements

The financial support by the Austrian Federal Ministry for Digital and Economic Affairs and the National Foundation for Research, Technology and Development and the Christian Doppler Research Association is gratefully acknowledged.

References

[1] P. Palensky and D. Dietrich. Demand side management: Demand response, intelligent energy systems, and smart loads. *Transactions in Industrial Informatics*, 7:381–388, 2011.

[2] M. Shafie-khah and P. Siano. Comprehensive review of the recent advances in industrial and commercial dr. *Transactions in Industrial Informatics*, 15:3757–3771, 2019.

[3] Q. Zhang and I. E. Grossmann. Planning and scheduling for industrial demand side management: Advances and challenges. *Alternative Energy Sources and Technologies: Process Design and Operation*, pages 383–414, 2016.

[4] A. Arteconi et al. State of the art of thermal storage for demand-side management. *Applied Energy*, 93:371–389, 2012.

[5] V. V. Tyagi and D. Buddhi. PCM thermal storage in buildings: A state of art. *Renewable and Sustainable Energy Reviews*, 11(6):1146–1166.

[6] B. Alimohammadisagvand et al. Cost-optimal thermal energy storage system for a residential building with heat pump heating and demand response control. *Applied Energy*, 174:275–287, 2016.

[7] A. Arteconi and F. Polonra. Demand side management in refrigeration applications. *International Journal of Heat and Technology*, 35:58–63, 2017.

[8] S. Shafiei et al. Modeling supermarket refrigeration systems for demand-side management. *Energies*, 6(2):900–920, 2013.

[9] F. L. Mueller et al. Power reference tracking of a large-scale industrial freezer system for ancillary service delivery. In *Innovative Smart Grid Technologies Europe (ISGT EUROPE), 2013 4th IEEE/PES*.

[10] P. Kepplinger et al. Autonomes demand side management verteilter energiespeicher. *e & i Elektrotechnik und Informationstechnik*, 2019.

[11] P. Kepplinger et al. Active demand side management with domestic hot water heaters using binary integer programming. In *e-nova*, volume 17, 2013.

[12] R. Kapoor and L. Metzger. Process cheese: Scientific and technological aspects - a review. *Comprehensive Reviews in Food Science and Food Safety*, 7:194–214, 2008.

[13] R. Heiss. *Lebensmitteltechnologie - Biotechnologische, chemische, mechanische und thermische Verfahren der Lebensmittelaufbereitung*. Springer-Verlag, Berlin, GER, 4.ed edition, 1991.
[14] Y. Edelby. *Strukturierungsmechanismen bei der Herstellung von Analog- und Schmelzkäse.* PhD thesis, Technische Universität Berlin, Berlin, GER, 2014.
[15] M. Moran et al. *Fundamentals of engineering thermodynamics*. John Wiley & Sons, Inc, seventh edition edition.
[16] *Planungshandbuch Dampfkessel*. Viessmann Group, Allendorf, GER.
[17] CDC, CDC - Climate Data Center Austria. `https://cdc.dwd.de/portal/`. [Online; accessed 10-Nov-2020].
[18] *Climaveneta - air cooled liquid chillers*. Climaveneta S.p.A., Italy, 2006.
[19] Matlab Release 2020a. The Mathswork, Inc., Natick, MA.
[20] A. Pajonk et al. Heat transfer study and modeling during emmental ripening. *Journal of Food Engineering*, 57:249–255, 2003.
[21] EXAA, EXAA - Energy Exchange Austria. `https://www.apg.at`. [Online; accessed 5-May-2021].